[14]N. F. Mott, Can. J. Phys. 34, 1356 (1956).
[15]W. F. Brinkman, T. M. Rice, P. W. Anderson, and S. T. Chui, Phys. Rev. Letters 28, 961 (1972).
[16]V. A. Gergel, Fiz. Tverd. Tela 11, 3538 (1969) [Sov. Phys. Solid State 11, 2962 (1970)].
[17]L. V. Keldysh and Yu. V. Kopaev, Fiz. Tverd. Tela 6, 2791 (1964) [Sov. Phys. Solid State 6, 2219 (1965)].
[18]E. O. Kane, J. Phys. Chem. Solids 1, 249 (1957).
[19]V. A. Gergel, R. F. Kazarinov, and R. A. Suris, Zh. Eksperim. i Teor. Fiz. 53, 544 (1967) [Sov. Phys. JETP 26, 354 (1968)].
[20]See, for instance, A. A. Abrikosov, L. P. Gor'Kov, and I. Ye. Dzyaloshinskii, *Quantum Field Theoretical Methods in Statistical Physics*, 2nd ed. (Pergamon, New York, 1965).
[21]We wish only to sketch the standard treatment. The reader interested in details, cautions, etc., is referred to a general text such as A. L. Fetter and J. D. Walecka, *Quantum Theory of Many Particle Systems* (McGraw-Hill, New York, 1971). Our notation should be understood as symbolic only; thus Matsubara sums have been indicated as energy integrals, etc., to avoid undue repetition of well-known details.
[22]B. I. Lundqvist, Physik Kondensierte Materie 6, 193 (1967); 6, 206 (1967); 7, 117 (1968).
[23]N. J. Horing has discussed the utility of the dielectric constant representation as unifying collective and microscopic descriptions of the quantum plasma in *Electronic Structures in Solids*, edited by E. D. Haidemenakis (Plenum, New York, 1969).
[24]This point may appear obvious, and it has received only cursory mention in Ref. 22; nevertheless, we stress it here since it is evidently not universally appreciated [cf. *Note added* to B. D. McCombe, R. J. Wagner, S. Teitler, and I. J. Quinn, Phys. Rev. Letters 28, 38 (1972)].
[25]N. J. Horing, Ann. Phys. (N.Y.) 31, 1 (1965).
[26]N. D. Mermin and E. Canel, Ann. Phys. (N.Y.) 26, 247 (1964).
[27]P. Nozières and D. Pines, Phys. Rev. 111, 442 (1958).
[28]Ya. Pokrovsky, Z. Kaminsky, and K. Svistunova, *Proceedings of the Tenth International Conference on the Physics of Semiconductors* (USAEC Div. Tech. Inf., Springfield, Va., 1970) (Conf-700801, Paper).
[29]W. D. Johnston, Jr., J. Appl. Phys. 42, 2731 (1971).
[30]R. J. Phelan, A. R. Calawa, R. H. Rediker, R. J. Keyes, and B. Lax, Appl. Phys. Letters 3, 143 (1963).
[31]F. L. Galeener, I. Melngailis, G. B. Wright, and R. H. Rediker, J. Appl. Phys. 36, 1574 (1965).
[32]F. L. Galeener, G. B. Wright, W. E. Krag, T. M. Quist, and H. J. Zeiger, Phys. Rev. Letters 10, 472 (1963).
[33]J. M. Hvam, Phys. Rev. B 4, 4459 (1971).
[34]K. L. Shaklee and R. F. Leheny, Appl. Phys. Letters 18, 475 (1971).
[35]W. T. Silfvast and J. S. Deech, Appl. Phys. Letters 11, 97 (1967).
[36]C. V. Shank, A. Dienes, and W. T. Silfvast, Appl. Phys. Letters 17, 307 (1970).
[37]N. Holonyak, Jr., D. R. Scifres, M. G. Craford, W. O. Groves, and D. L. Keune, Appl. Phys. Letters 19, 256 (1971).
[38]R. E. Nahory, K. L. Shaklee, R. F. Leheny, and R. A. Logan, Phys. Rev. Letters 27, 1647 (1971).
[39]N. Holonyak, Jr., D. R. Scifres, H. M. Macksey, R. D. Dupuis, Y. S. Moroz, C. B. Duke, G. G. Kleiman, and F. V. Williams, Phys. Rev. Letters 28, 230 (1972).

PHYSICAL REVIEW B VOLUME 6, NUMBER 4 15 AUGUST 1972

Electronic Band Structure and Optical Properties of 3*C*-SiC, BP, and BN

L. A. Hemstreet, Jr.* and C. Y. Fong
Department of Physics, University of California, Davis, California 95616
(Received 22 February 1972)

The energy band structure and optical properties of the zinc-blende semiconductors 3*C*-SiC, BP, and BN have been calculated using a nonlocal version of the empirical-pseudopotential method. The results of this investigation are discussed and compared to experiment. The agreement between theory and experiment is found to be very good for both SiC and BP. The BN results are quite rough, owing to some very questionable assumptions made necessary because of the scarcity of experimental data. However, the results seem to give a reasonable first approximation to the correct band structure. The effect of the nonlocal p pseudopotential on these three crystals is discussed.

I. INTRODUCTION

During the last several years, the empirical-pseudopotential method (EPM) has been successfully used by many authors to gain valuable insight into the band structure and optical properties of a large group of semiconductors.[1] This method of calculation has been applied to the group-IV elements C, Si, Ge, and α-Sn, which crystallize in the diamond structure, as well as to many of the III-V and II-VI compounds, most of which exhibit the zinc-blende crystal structure. We report here the results of applying the EPM to 3*C*-SiC, BP, and BN. Since the materials discussed in this work are of interest as potential solid-state devices due to their high melting point, chemical inertness,

and high hardness, it is hoped that these results will serve to help establish some of their important physical properties.

In general, the EPM calculations give best results for those solids which satisfy the conditions of the so-called cancellation theorem.[2] Namely, that there exist in the solid core states of the same l as those of the valence states present; e.g., if the solid under investigation has valence states with s and p characters, the core states should also contain s-like and p-like states. Under these conditions the one-electron pseudopotential V_p composed of the usual attractive crystal potential plus a repulsive term arising from the orthogonality of the valence wave functions to the core states will be very weak. If one then expands $V_p(\vec{r})$ in reciprocal-lattice vectors, one needs to keep only the first few terms in the expansion as higher terms should be small due to the cancellation effect. This being the case, the band structure of the solid depends only on a small number of parameters, the first few coefficients (called form factors) of the expansion of $V_p(\vec{r})$ in reciprocal-lattice vectors. In the EPM, one treats these form factors as parameters to be determined by available experimental data, as discussed in Sec. III and more fully in the recent article by Cohen and Heine.[1]

Most of the group-IV solids, as well as the III-V and II-VI compounds, considered thus far have satisfied the cancellation theorem, and the results have been quite good. Almost all of the solids have s and p core states to compensate the crystal potential seen by s- and p-like valence electrons. Exceptions to this trend occur when the solid contains elements from row 1 of the Periodic Table, such as boron, carbon, or nitrogen. For these elements, the core contains no p states and hence the p-like valence states feel the full crystal potential in the core region. As a result, one would not except to be able to keep just the first few terms in the expansion of $V_p(\vec{r})$ for p states, and the EPM would not be expected to yield good results for these solids. Actually, the EPM calculations of diamond[3,4] work reasonably well and seem to give band gaps which are roughly correct and a conduction-band minimum which is consistent with experiment. This success is probably due to the fact that the p electrons are not normally found in the core region very much, anyway, due to the asymmetry of the wave function. However, $\epsilon_2(\omega)$ calculations[4] which test the band structure over a fairly wide range of energies have been disappointing.

In an effort to improve the results of calculations involving solids with elements from row 1, we have modified the EPM by adding to the pseudopotential $V_p(\vec{r})$ a nonlocal, angular-momentum-dependent potential V_{NL}, which acts only on p states, to account for the fact that the p-like valence electrons see the entire crystal potential in the core region, and not a weak pseudopotential. With the addition of this term, one can again expand $V_p(\vec{r})$ in terms of only a few reciprocal-lattice vectors, obtaining a small set of parameters. These can be combined with a very small number of parameters coming from V_{NL}, and fit to experiment as before. Such a scheme was used to investigate the properties of diamond and the results have been published.[5] The $\epsilon_2(\omega)$ spectrum resulting from this nonlocal-empirical-pseudopotential method (NEPM) seems to give much better agreement with experiment than does the EPM results obtained without V_{NL}. In this paper, we shall extend the NEPM analysis to the IV-IV compound 3C-SiC and the III-V compounds BP and BN, all of which crystallize in the zinc-blende structure.

The paper will be presented in six sections. Section II briefly describes the calculational procedure employed in determining the energy bands and optical properties of these solids using the NEPM. In Sec. III we discuss the band structure and optical properties of 3C-SiC. The band structure has already been discussed in a previous paper,[6] so we concentrate on the optical properties in this section. We also include the band structure calculated without the nonlocal term $V_{NL}(\vec{r})$, and show that the nonlocal effects are not as important as they were in diamond. We then turn our attention to BP in Sec. IV, where we discuss the band structure and optical properties and compare them to those of 3C-SiC. Boron nitride is covered in Sec. V. In this section we discuss some rather drastic assumptions we make about the BN form factors, made necessary due to the scarcity of reliable experimental data. We show that the resulting band structure is probably a rough, but nevertheless reasonable, first approximation to the real thing, and discuss ways in which it might be improved. Finally, Sec. VI presents some conclusions derived from this investigation.

II. CALCULATIONAL PROCEDURE

The electronic-energy-band structure and wave functions of the compounds SiC, BP, and BN are calculated using the empirical pseudopotential method (EPM), modified to account for the lack of p states in the C, B, and N cores. The calculational procedure is quite similar to that described in HFC.[5] Briefly, one starts from the Hamiltonian

$$H=\frac{p^2}{2m}+\sum_{|\vec{G}|^2\leq 11} V_p(\vec{G})e^{i\vec{G}\cdot\vec{r}}+V_{NL}(\vec{r}), \tag{1}$$

where the pseudopotential $V_p(\vec{r})$ is expanded in reciprocal-lattice vectors, and the nonlocal term $V_{NL}(\vec{r})$ is added to account for the lack of cancellation of the full crystal potential for p valence states in the C, B, or N core regions. With the addition

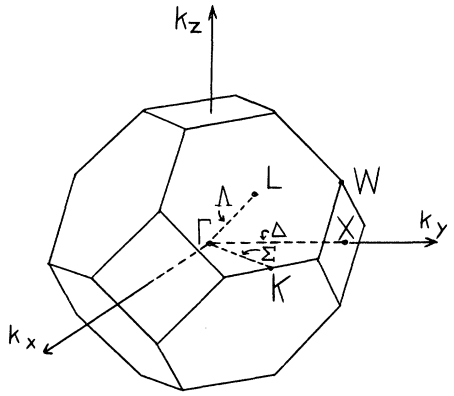

FIG. 1. First BZ of the fcc crystal lattice.

of this term, one needs to retain only the first few terms in the expansion of $V_p(\vec{r})$; we have kept only those reciprocal-lattice vectors which have $G^2 \leq 11$, where G is measured in units of $2\pi/a$, a being the appropriate lattice constant ($a = 4.35$ Å for SiC, $a = 5.43$ Å for BP, and $a = 3.615$ Å for BN). As in our calculation of diamond, $V_{\rm NL}(\vec{r})$ is taken to have the form

$$V_{\rm NL}(\vec{r}) = \sum_n \hat{P}_1^\dagger U_{\rm NL}(|\vec{r} - \vec{R}_n|)\hat{P}_1, \tag{2}$$

where $\hat{P}_1$ is a projection operator which acts only on states with $l = 1$, $\hat{P}_1^\dagger$ is the Hermitian conjugate of $\hat{P}_1$, and

$$U_{\rm NL}(|\vec{r} - \vec{R}_n|) = \begin{cases} A_m r e^{-\alpha_m r}, & r \leq R_c \\ 0, & r > R_c \end{cases}. \tag{3}$$

The sum over n includes only those ion cores without p states, and the A_m, α_m, where the subscript m labels the B, N, or C cores, are treated as parameters. R_c is chosen to have the average value of 0.2 Å for all of the compounds considered here.

All three solids, 3C-SiC, BP, and BN, crystallize in the zinc-blende structure, which consists of an fcc lattice with a basis. The first Brillouin zone (BZ) for this structure is shown in Fig. 1, with important symmetry points and directions indicated. We shall employ the notation of Parmenter[7] throughout in the labeling of both the symmetry points and the irreducible representations of the point group. If the origin of coordinates is chosen to lie midway between the two atoms forming the basis, these atoms will be situated at positions $\pm\vec{\tau} = \pm\frac{1}{8}a(1, 1, 1)$ in the unit cell, where a is the appropriate lattice constant.

Unlike the diamond structure, zinc-blende crystals do not possess inversion symmetry. It is convenient to decompose the Fourier coefficients $V_p(\vec{G})$ into parts which are symmetric and antisymmetric under such an inversion as follows:

$$V_p(\vec{G}) = V_s(\vec{G})\cos\vec{G}\cdot\vec{\tau} + iV_A(\vec{G})\sin\vec{G}\cdot\vec{\tau}, \tag{4}$$

where

$$2V_S(\vec{G}) = v_1(\vec{G}) + v_2(\vec{G}), \tag{5}$$

$$2V_A(\vec{G}) = v_1(\vec{G}) - v(\vec{G}), \tag{6}$$

and

$$v_1(\vec{G}) = (2/\Omega_0)\int_{\rm cell} v_1(\vec{r})e^{-i\vec{G}\cdot\vec{r}}d^3r \tag{7}$$

is the crystal form factor for an atom of type 1, with an analogous expression for $v_2(\vec{G})$, the crystal form factor for atoms of type 2. This decomposition of the pseudopotential form factors $V_p(\vec{G})$ into symmetric and antisymmetric parts, each of which is itself written as the product of a structure factor, which depends only on the positions of the ion cores in the solid, and a crystal form factor, which is independent of the ion position is a standard procedure in the investigation of zinc-blende solids. In these definitions, Ω_0 is the volume of the unit cell ($\Omega_0 = \frac{1}{4}a^3$ for the fcc structure), and the intregrals in (7) are done over the unit cell volume. It should be noted that the crystal form factors, as defined by (7), are normalized to volume per atom in the solid.

The energy band structure and pseudo-wave functions are obtained by diagonalizing H, using Eqs. (2)–(4), over a basis of plane wave states. In addition we use a form of perturbation theory described by Brust.[8] Essentially, one treats those plane waves with $|\vec{k}+\vec{G}|^2 \leq E_1$ exactly, while those such that $E_1 < |\vec{k}+\vec{G}|^2 \leq E_2$ enter via second-order perturbation theory.[8] Plane waves with $|\vec{k}+\vec{G}|^2 > E_2$ are neglected. E_1 and E_2 are chosen to give reasonable convergence to the energy eigenvalues, ~0.05 eV. We neglect the contribution of those plane waves with $E_1 < |\vec{k}+\vec{G}|^2 \leq E_2$ for the nonlocal potential. Satisfactory convergence for 3C-SiC and BP is obtained by choosing $E_1 = 10.5$ and $E_2 = 27.0$. This corresponds to an expansion of the wave function in approximately 30 plane waves, with another 150 or so entering via second-order perturbation theory. For BN, it was necessary to increase E_1 to 12.0 and E_2 to 31.0, resulting in about 50 plane waves entering the expansion via first order, with another 130 or so entering via second-order theory.

A typical matrix element of $V_{\rm NL}$ is of the form

$$V^{\rm NL}_{\vec{G}\vec{G}'} = (48\pi/a^3)\cos\theta_{\vec{G}\vec{G}'}[(I^{(1)}_{\vec{G}\vec{G}'} + I^{(2)}_{\vec{G}\vec{G}'})\cos(\vec{G}-\vec{G}')\cdot\vec{\tau} + i(I^{(1)}_{\vec{G}\vec{G}'} - I^{(2)}_{\vec{G}\vec{G}'})\sin(\vec{G}-\vec{G}')\cdot\vec{\tau}], \tag{8}$$

where

$$I_{\vec{G}\vec{G}'} = \int_0^{R_c} j_1(|\vec{k}+\vec{G}'|r)j_1(|\vec{k}+\vec{G}|r)Ae^{-\alpha r}r^3dr, \tag{9}$$

j_1 is the spherical Bessel function of order 1, and $\theta_{\vec{G}\vec{G}'}$ is the angle between the vectors $|\vec{k}+\vec{G}\rangle$ and $|\vec{k}+\vec{G}'\rangle$.

Once the energy band structure and the wave functions are obtained, $\epsilon_2(\omega)$, the imaginary part of the dielectric response function, is determined via the relation

$$\epsilon_2(\omega) = \frac{e^2\hbar^2}{m} \sum_{v,c} \frac{1}{(2\pi)^3} \int_S \frac{f_{vc}(\vec{k})\, ds}{E_{vc} |\nabla_{\vec{k}} E_{vc}|}, \tag{10}$$

where

$$f_{vc}(\vec{k}) = \frac{2}{3m} \frac{|\langle \vec{k}, v | \vec{p} | \vec{k}, c \rangle|^2}{E_{vc}} \tag{11}$$

is the EPM interband oscillator strength, $|\vec{k}, c\rangle$ and $|\vec{k}, v\rangle$ are the EPM wave functions for the conduction and valence states, respectively, at the point $\vec{k}$ in the BZ, S is a surface of constant-interband-energy $E_{vc} = E_c - E_v$, E_v and E_c are the valence and conduction band energies, respectively, and m and e represent the electron mass and charge. The method of computing the sums is described in HFC. One can obtain the reflectance $R(\omega)$ from $\epsilon_2(\omega)$ by using the Kramers-Kronig relation to find $\epsilon_1(\omega)$, the real part of the dielectric constant, and then using

$$R(\omega) = \frac{(\epsilon_1^2+\epsilon_2^2)^{1/2} - [2\epsilon_1 + 2(\epsilon_1^2+\epsilon_2^2)^{1/2}]^{1/2} + 1}{(\epsilon_1^2+\epsilon_2^2)^{1/2} + [2\epsilon_1 + 2(\epsilon_1^2+\epsilon_2^2)^{1/2}]^{1/2} + 1}, \tag{12}$$

as described in a paper by Walter and Cohen.[9]

From Eqs. (1)–(4), one sees that the energy band structure and wave functions of the compounds 3C-SiC, BP, and BN are completely determined by the small set of parameters $[V_A(\vec{G}), V_S(\vec{G}), G^2 \leq 11, A_m, \alpha_m]$ in this scheme. For the zinc-blende structure, the only values of $V(\vec{G})$ with $G^2 \leq 11$ are those corresponding to $G^2 = 3, 4, 8, 11$. Further, $\sin\vec{G}\cdot\vec{\tau} = 0$ for $G^2 = 8$, and $\cos\vec{G}\cdot\vec{\tau} = 0$ for $G^2 = 4$. Hence a knowledge of the six local-form-factors $[V_s(G^2 = 3), V_S(8), V_S(11), V_A(3), V_A(4), V_A(11)]$, plus the nonlocal parameters A, α enables one to compute the band structure and optical constants of these compounds. In the NEPM scheme, one uses experimental optical data to determine these parameters. The procedure is described in detail in a recent review article by Cohen and Heine.[1] Figure 2 summarizes the steps. One first makes a guess at the parameters, either by extrapolating from nearby compounds, as in the case of BP and BN, or by scaling previous results for the constituent elements, as in SiC. In either case, one uses these parameters to calculate energy gaps at selected $\vec{k}$ values in the BZ. These are then compared to values extrapolated from experimental data in a manner described by Phillips[10] and Cohen and Heine.[1] The form factors are then adjusted until satisfactory agreement with those values obtained from the experimental data is reached. Then one calculates $\epsilon_2(\omega)$ and $R(\omega)$ and compares them to the experimental spectra. If agreement is again satisfactory, one interprets the optical spectra, etc., in terms of

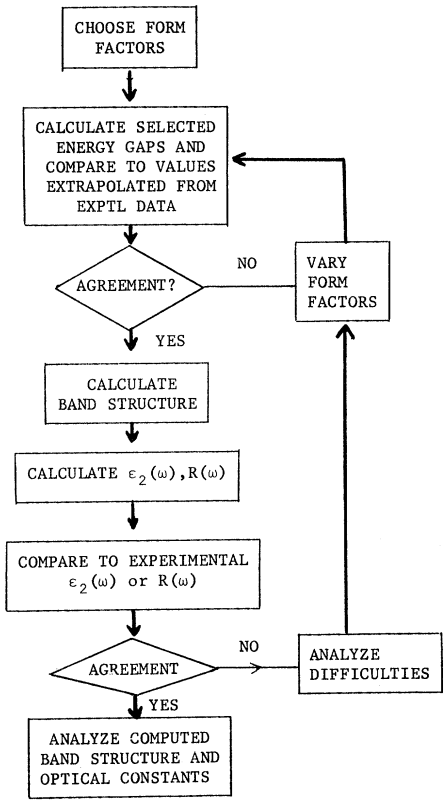

FIG. 2. Schematic outline of the EPM calculational procedure.

the computed band structure. If not, one repeats the process until, hopefully, agreement is reached. Clearly, the more one knows about the band structure, and the more accurate the experimental data, the faster the process and the better the results. In the next sections, we shall discuss the results of these calculations, including the choice of parameters and the resulting band structures and optical constants, for SiC, BP, and BN separately.

III. 3C-SiC

The choice of parameters $V_S(G^2)$, $V_A(G^2)$, A, α has been discussed previously in Ref. 6 (hereafter to be referred to as I). Briefly, initial values of the local parameters $V_S(G^2)$, $V_A(G^2)$ are determined by combining the diamond form factors of HFC with the silicon form factors of Brust,[8] each having been scaled to account for the difference in lattice constant between 3C-SiC and C and Si, respectively. The nonlocal parameters A, α, which refer to only the carbon ion cores, are taken to retain the same values which they have in the diamond lattice, but scaled by a factor of a_C/a_{SiC} to account for the differing lattice constant of the two solids. The local parameters (V_S, V_A) are then allowed to vary, with A, α held fixed, until satis-

TABLE I. Parameters used in the calculation of the band structure of 3C-SiC, BP, and BN. The form factors are given in Ry.

Form factors	3C-SiC	BP	BN
$V_s(G^2=3)$	−0.419 Ry	−0.373 Ry	−0.79 Ry
$V_s(8)$	0.101	0.085	0.19
$V_s(11)$	0.118	0.099	0.14
$V_A(3)$	0.001	0.010	0.06
$V_A(4)$	0.08	0.023	0.08
$V_A(11)$	0.051	0.034	0.02
A	−0.128	−0.09	−.16
α	$1.02A^{-1}$	$1.04A^{-1}$	$1.28A^{-1}$
E_1	10.0	10.5	12.0
E_2	27.0	27.0	31.0
a	4.35 Å	5.43 Å	3.615 Å

factory agreement with experiment is reached, as discussed in Sec. II. The final choice of parameters resulting from this procedure is reproduced in Table I for convenience.

The band structure resulting from the use of the parameters in Table I is shown in Fig. 3. Also shown (dashed line) is the band structure of 3C-SiC calculated using the same local parameters $V_S(G^2)$, $V_A(G^2)$, but with $A=0$ (i.e., no nonlocal potential term added). It should be noted that the band structure shown in Fig. 3 is not identical to the band structure reported in I. The reason for this is that there was a slight error in the computer code used to calculate the band structure reported in I, which resulted in some (not all) of the matrix elements of the antisymmetric part of the nonlocal potential having the wrong sign. This introduced erroneous shifts in some (but again, not all) of the energy levels at various points in the BZ. For the most part, such shifts are insignificant, being $\lesssim 0.05$ eV. Moreover, the energy gaps change even less, the difference usually being $\lesssim 0.02$ eV. However the shifts are somewhat larger for some of the bands at X, Γ. The largest difference between the corrected band structure of Fig. 3 and that reported in I occurs in the lowest-lying valence band (band 1) in the region about X and extending out toward K. The corrected energy of X_{1v} is about 0.17 eV greater than that shown in I. The rest of band 1 is essentially the same in both cases. There is also a shift of 0.10 eV introduced into the energy of Γ_{1c} (band 5), and a shift of 0.12 eV at X_{5c} (bands 7, 8 at X). Both of these corrections are rather localized about the symmetry points mentioned, with the remainder of the band structure essentially unaffected. With these three exceptions, the band structure of Fig. 3 is identical to that reported in I.

As one can see from Fig. 3, 3C-SiC is an indirect-gap material with valence-band maximum at Γ_{15v} and conduction-band minimum at X_{1c}. The calculated threshold for indirect transitions is 2.33 eV, corresponding to the $\Gamma_{15v}-X_{1c}$ transition.

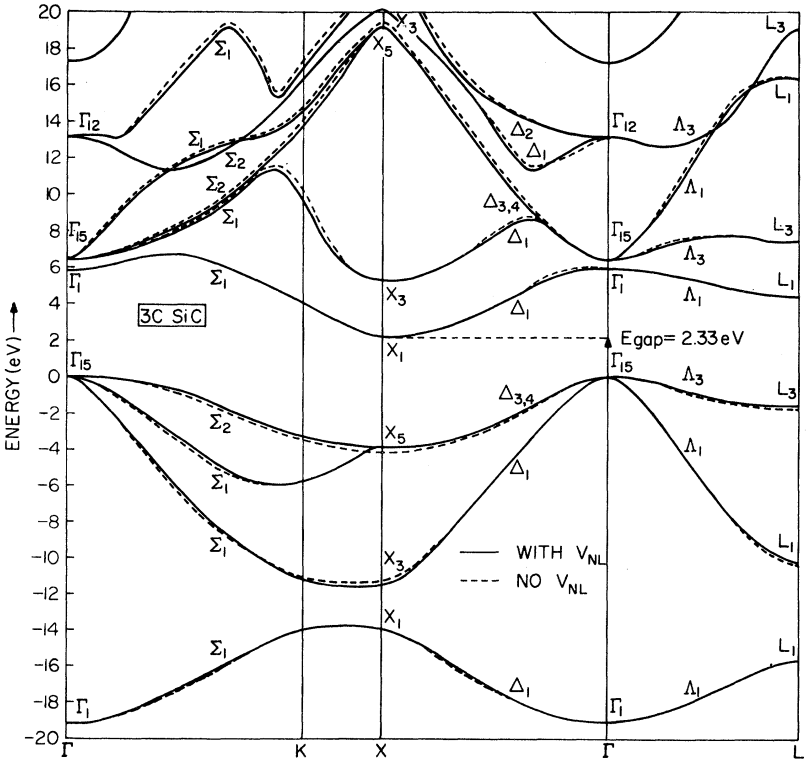

FIG. 3. Energy band structure of 3C-SiC, both with (full line) and without (dashed line) the inclusion of V_{NL}.

TABLE II. Key energy gaps of 3C-SiC, BP, and BN both with and without V_{NL}, at selected symmetry points in the BZ.

Solid	Γ_{15}-Γ_1 (eV)	Γ_{15}-Γ_{15} (eV)	L_3-L_1 (eV)	L_3-L_3 (eV)	X_5-X_1 (eV)	X_5-X_3 (eV)	Γ_{15}-L_1 (eV)	Γ_{15}-X_1 (eV)
SiC	5.90	6.47	5.97	9.08	6.13	9.21	4.39	2.33
SiC (no V_{NL})	5.92	6.49	6.02	9.18	6.37	9.40	4.38	2.35
BP	5.25	5.38	5.0	8.02	6.07	7.34	3.40	2.18
BP (no V_{NL})	5.22	5.39	5.04	8.13	6.31	7.55	3.34	2.19
BN	8.36	10.83	9.88	14.95	12.69	13.75	7.62	7.60
BN (no V_{NL})	8.51	11.04	9.95	15.25	13.10	14.18	7.55	7.69

This is in good agreement with the experimental value of 2.39 eV determined by Choyke, Hamilton, and Patrick.[11] The threshold for direct transitions is 5.90 eV, associated with the Γ_{15v}- Γ_{1c} transition.

A listing of band energies at selected symmetry points in the BZ, calculated both with and without $V_{NL}(\vec{r})$, is shown in Table II. As one can see from these tables and from the band structure itself, the effect of the nonlocal term V_{NL} is to shift the energy bands slightly, the largest effect being a shift of 0.23 eV in the highest valence band (band 4) at X. $V_{NL}(\vec{r})$ has its major effect on band 4 in the region near X, and extending out above the Δ direction toward Γ, and out along Σ toward K, where energy shifts are all between 0.15–0.25 eV. As expected, V_{NL} has virtually no effect on the lowest conduction band (band 5), which has little or no p-like character. Thus, V_{NL} has its major influence on 4 → 5 transitions, which are the major contributions to $\epsilon_2(\omega)$ for energies less than or equal to that of the main peak, in the region of the BZ near X, extending out along Δ toward Γ, and also out along Σ to K. But this is just the region in $\vec{k}$ space which contributes most strongly to the main peak in the reflectivity spectra of III-V and IV-IV compounds and group-IV solids, as was pointed out in our previous discussion on diamond in HFC, and as will be shown to be true for 3C-SiC and BP as well. The effect of the nonlocal term in 3C-SiC is much less important than it was for diamond, where energy shifts as large as 0.75 eV or so were found, and could probably be omitted. A very rough calculation of $\epsilon_2(\omega)$, using only about 250 000 sampling points in the BZ instead of the usual 10^6 or so, indicates that the effect of V_{NL} is merely to shift the entire $\epsilon_2(\omega)$ spectrum by approximately 0.2 eV, without introducing any new features. This shift could possibly be all or partially compensated for by appropriate changes in $[V_S(G^2), V_A(G^2)]$. Such is not the case for diamond however, where the inclusion of $V_{NL}(\vec{r})$ is absolutely necessary in order for the main $\epsilon_2(\omega)$ peak at 12.0 eV to be accurately reproduced.

Arguments for the accuracy of the band structure of Fig. 3 have already been advanced in I and will not be repeated here. Instead, we shall concentrate on a discussion of the optical properties of the solid as manifested in $\epsilon_2(\omega)$, the imaginary part of the dielectric response function, and in $R(\omega)$, the reflectance. The calculated $\epsilon_2(\omega)$ of 3C-SiC, obtained by using Eq. (10) with the NEPM wave functions and band structure of Fig. 3, is shown in Fig. 4, while the reflectance, derived via a Kramers-Kronig transformation on $\epsilon_2(\omega)$ as described in Sec. III, is shown in Fig. 5. Also presented in Fig. 5 is the experimental results of Wheeler[12] (dashed line). Important energy contours and critical points are presented in Figs. 6 and 7 for 4 → 5 and 4 → 6 interband transitions, respectively.

As can be seen from Fig. 5, the experimental $R(\omega)$ spectrum has prominent structure at 4.6, 6.0, 7.1, 7.8, 8.3, and 9.7 eV. The theoretical $R(\omega)$ spectrum has corresponding structure at 6.2, 6.8, 7.9, 8.5, 9.5, and 10 eV. The agreement between the two curves is quite good, except that the calculation does not reproduce the 4.6-eV edge in the beginning of the spectrum, and it shows a doublet structure in the range 9.5–10 eV instead of the single peak at 9.7 eV observed by Wheeler.

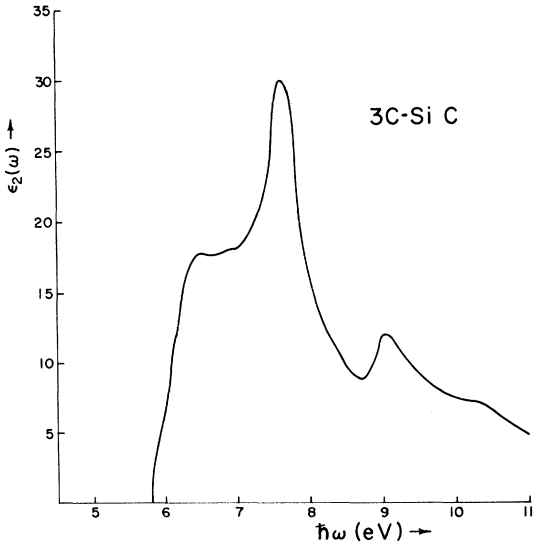

FIG. 4. Theoretical $\epsilon_2(\omega)$ of 3C-SiC.

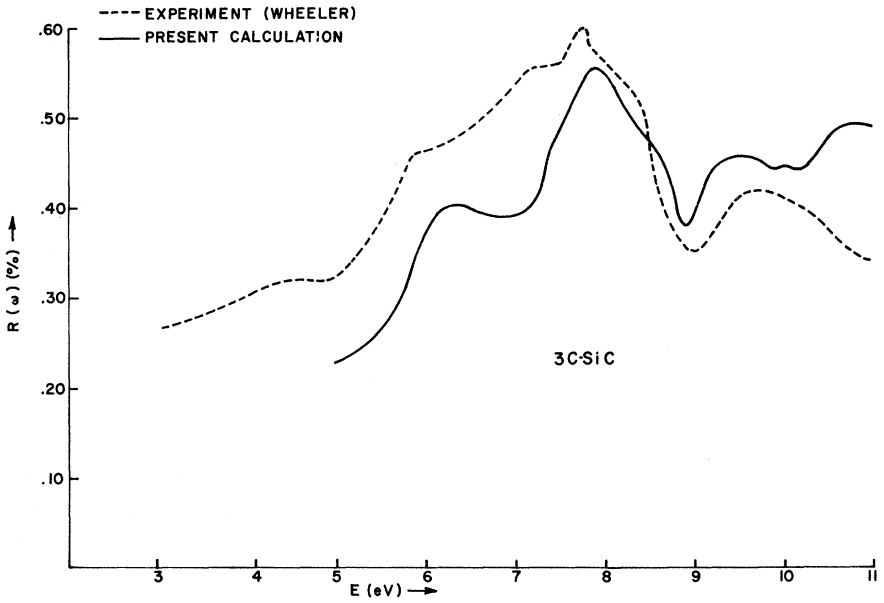

FIG. 5. Reflectance spectra of 3C-SiC. The full line shows the calculated result, while the dashed line indicates the experimental results of Wheeler (Ref. 12).

However, it should be noted that the 4.6-eV edge was not observed in independent measurements made by Choyke and Patrick,[13] who report no structure below 6.0 eV, which they identify to be the fundamental gap for direct transitions. Thus, there is some doubt as to the reliability of this 4.6-eV edge in Wheeler's results. We have chosen our parameters so that the resulting band structure of 3C-SiC has a fundamental gap for direct transitions near 6.0 eV, which are in agreement with the measurements of Choyke and Patrick. As for the doublet structure in the 9.5–10-eV region, it is interesting to note that the experimental results of Belle *et al.*[14] do report a doublet in this region instead of the single peak, and a previous calculation of $\epsilon_2(\omega)$ made by Herman *et al.*[15] also predicts such a doublet structure. Hence this result must also be considered somewhat uncertain at this time. Outside of these two exceptions, however, the two $R(\omega)$ spectra seem to agree very well indeed.

In order to determine the interband transitions responsible for the structure in $R(\omega)$, it is convenient to study $\epsilon_2(\omega)$, which directly depends on interband transitions within the BZ. One cannnot directly compare the positions of structure in $\epsilon_2(\omega)$ and $R(\omega)$ due to the fact that the Kramers-Kronig transformation introduces energy shifts of 0.1–0.5 eV between the two, but the fact that the theoretical $R(\omega)$ seems to agree so well with experiment would indicate that the corresponding $\epsilon_2(\omega)$ from which it was derived should also be accurate.

The $\epsilon_2(\omega)$ spectrum of Fig. 4 has structure at 6.0, 6.2, 6.5, 6.9, 7.6, 8.3, 9.1, and 9.9 eV. The spectrum begins with direct transitions at Γ of energy 5.90 eV, corresponding the $\Gamma_{15v} - \Gamma_{1c}$ transition. This M_0 critical point provides the threshold for the structure near 6 eV. As more and more points in the BZ begin to contribute, $\epsilon_2(\omega)$ rises rapidly. Reference to Fig. 6 shows that contributions to $\epsilon_2(\omega)$ in the region about 6 eV come mainly from $4 \rightarrow 5$ transitions near Γ, L, X, which are very close in energy, and along the Λ direction from Γ to L, where bands 4, 5 are essentially parallel. The matrix elements are quite large in this region of $\vec{k}$ space as well. The weak edges at 6.0 and 6.2 can be assigned to M_0 critical points at L associated with the $L_{3v} - L_{1c}$ transition (5.97 eV), and X, where the $X_{5v} - X_{1c}$ energy gap is 6.13 eV, respectively. In addition, there is an M_1 critical point near $(2\pi/a)(0.1, 0.1, 0.1)$ with energy 6.10 eV. All of these critical points probably contribute to the 6.0-eV peak in the experimental reflectivity spectrum of Wheeler.

The shoulder in $\epsilon_2(\omega)$ at 6.5 eV can be identified with an M_0 singularity at Γ corresponding to the $4 \rightarrow 6$ transition $\Gamma_{15c} - \Gamma_{15v}$ of energy 6.47 eV. In addition, there is a point of inflection in the $4 \rightarrow 6$ energy plane near the point $(2\pi/a)$ (0.40, 0, 0), which has energy 6.43 eV. This has some effect as a weak pair of critical points of the M_0 and M_1 variety. The edge at 6.9 eV does not seem to be associated with any critical points, but seems to be a volume effect due mainly to $4 \rightarrow 5$ transitions throughout the BZ, as shown in Fig. 6.

The large central peak at 7.6 eV in $\epsilon_2(\omega)$, corresponding to the 7.8-eV peak in the experimental $R(\omega)$, is predominantly a volume effect, even though there is an M_2 singularity on the Σ axis near $(2\pi/a)$ (0.50, 0.50, 0), with an energy gap of 7.76

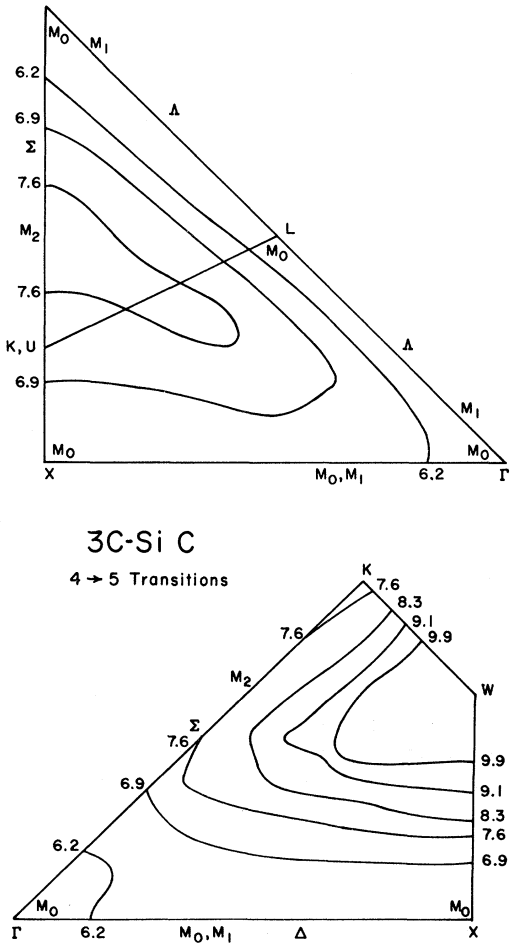

FIG. 6. Important 3C-SiC energy contours and critical points for 4–5 transitions.

eV. This large peak in the spectra of III-V, IV-IV, and group-IV materials has often been called the X peak, and has been assumed to result from nearly degenerate critical points at X and Σ of the M_1 and M_2 type, respectively. While such critical points often accompany this peak, these are not absolutely necessary to explain its presence, as shown here, where the X gap lies almost 1.5 eV below the main peak, and as shown in diamond, where there is no critical point at Σ. In addition, it was found during the course of our investigation of diamond that the position of the main peak in $\epsilon_2(\omega)$ does not always agree with the energy of the $4 \rightarrow 5$ gap at X ($X_4 - X_1$); often, differences of as much as 1 eV or so were observed. What does seem to be the most important factor in determining the main peak of the optical spectrum are $4 \rightarrow 5$ transitions in the BZ, especially in the ΓXWK plane near K and extending along the Σ direction toward Γ as shown in Fig. 6. In addition to getting contributions from a large region in $\vec{k}$ space, the matrix elements in this region are very large and hence the contribution to $\epsilon_2(\omega)$ is quite significant. There are also contributions from $4 \rightarrow 6$ transitions as shown in Fig. 7. However, these $4 \rightarrow 6$ contributions to the main peak are less than 10% of the whole; the major contributors are the $4 \rightarrow 5$ transitions from the regions in the ΓXWK plane just discussed.

Above 7.6 eV, $4 \rightarrow 6$ contributions become more and more important. Since the elements for such transitions are usually smaller than for $4 \rightarrow 5$ transitions, $\epsilon_2(\omega)$ begins to fall smoothly as energy increases. The weak shoulder at 8.3 eV seems to be a volume effect, arising mainly from $4 \rightarrow 5$ transitions, as shown in Fig. 6, but with $3 \rightarrow 5$ and $4 \rightarrow 6$ transitions contributing as well. The peak at 9.1 arises from an M_0 singularity at L corresponding to the $4 \rightarrow 6$ ($L_{3v} - L_{3c}$) transition of 9.06 eV, combined with another critical point of the M_0 type at X associated with the $X_{5v} - X_{3c}$ transition of energy 9.20 eV. In addition, there is a fairly large $4 \rightarrow 6$ energy contour corresponding to the energy 9.1

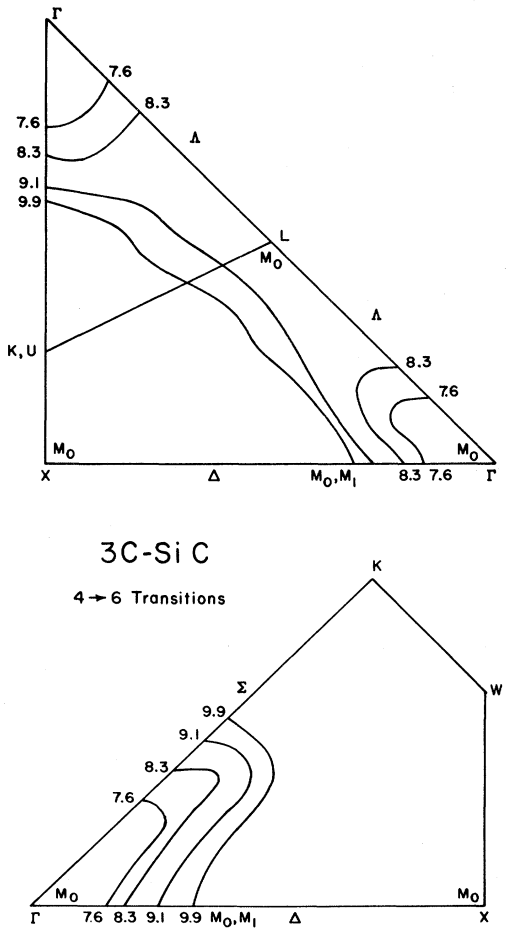

FIG. 7. Important 3C-SiC energy contours and critical points for 4–6 transitions.

TABLE III. Summary of optical structure, with associated critical points, for 3C-SiC. The experimental energies are taken from the reflectance spectrum of Wheeler (Ref. 12), while the theoretical energies are taken from the calculated $\epsilon_2(\omega)$ spectrum, with the corresponding energy in the reflectance spectrum shown in parentheses immediately following.

Energy of optical structure (eV)		Associated critical points		
Expt.	Theoret.	Interband transition	Symmetry	Energy (eV)
6.0	6.0(6.2)	Γ_{15v}-Γ_{1c}	M_0	5.90
		L_{3v}-L_{1c}	M_0	5.97
7.1	7.3	Volume effect		
7.8	7.6(7.9)	Σ_{2v}-Σ_{1c}	M_2	7.78
8.3	8.3(8.1)	Volume effect		
9.7	9.1(9.5)	L_{3v}-L_{3c}	M_0	9.06
		X_{5v}-X_{3c}	M_0	9.20
	9.9	Volume effect		

eV, as shown in Fig. 7. The very small peak at 9.9 eV has no associated critical points, and may be due to sampling procedure used in calculating $\epsilon_2(\omega)$.

We have summarized the experimental optical structure of 3C-SiC in Table III, where we have also listed associated critical points and the corresponding interband transitions. The position of the experimental structure is taken from the $R(\omega)$ spectrum of Wheeler. The theoretical energy is taken from the calculated $\epsilon_2(\omega)$ spectrum of Fig. 4 with the corresponding position in the calculated $R(\omega)$ listed in parentheses immediately following. This information will be very useful when we wish to compare the spectra of 3C-SiC, BP, and BN.

IV. BP

To determine the band parameters for BP, it is convenient to think of BP as derived from 3C-SiC by a replacement of the silicon atoms by phosphorous and the carbon atoms by those of boron. This being the case, one would expect the symmetric form factors $[V_S(3),\ V_S(8),\ V_S(11)]$ of BP to be roughly the same as those of 3C-SiC, properly scaled to account for the difference in lattice size, of course. The antisymmetric form factors $[V_A(3),\ V_A(8),\ V_A(11)]$ are expected to differ due to the difference in core charges between boron and phosphorous. Thus, as a starting point in determining these parameters, we choose them to have the scaled 3C-SiC values, and then allow the antisymmetric form factors $[V_A(3),\ V_A(4),\ V_A(11)]$ to vary freely to fit the optical data, keeping the nonlocal parameters $\{A, \alpha\}$ fixed, and allowing the symmetric parameters $[V_S(3),\ V_S(8),\ V_S(11)]$ to vary slightly, within ± 0.02 Ry or so, to account for possible errors of 0.1–0.3 eV in fitting the optical spectra of 3C-SiC. In this scheme, one has three free parameters with which to fit the optical data of BP, while another three can be varied slightly if needed. The final choice of parameters is given in Table I, alongside those of 3C-SiC. It is interesting to note that the antisymmetric form factors of BP are all quite small, the largest being 0.03 Ry, indicating that BP is essentially purely covalent. This agrees with the results of lattice infrared spectra reported by Gielisse *et al.*,[16] whose reflectivity measurements suggest a very low effective charge ($e^* \simeq 0.25e$), indicating BP to be the most covalent of the III-V compounds studied thus far. This is further corroborated by the quantum dielectric theory of electronegativity in covalent systems developed by Phillips and Van Vechten,[17] who have determined the fraction of ionic character of BP to be less than 1%.

The antisymmetric form factors of 3C-SiC, like those of BP, are very small for $G^2 \leq 3$. However, for higher values of G^2, they become very much larger than those of BP, especially in the region $5 \leq G^2 \leq 10$, where the values are all in the range 0.15–0.20 Ry. By way of contrast, the antisymmetric form factors of BP are uniformly small, never getting greater than 0.05 Ry or so. This implies that 3C-SiC should be more ionic in character than in BP, a fact confirmed both by lattice reflectivity measurements, which suggest a larger effective charge for 3C-SiC ($e^* \sim 0.5e$), and by the quantum dielectric theory of Van Vechten and Phillips, who calculate the fraction of ionic character of 3C-SiC to be close to 20%.

The energy band structure of BP derived from the parameters in Table I is shown in Fig. 8. BP, like 3C-SiC, is found to be an indirect gap material with valence band maximum at Γ, and conduction band minimum at X_{1c}. The calculated value of the $\Gamma_{15v} - X_{1c}$ indirect gap is 2.18 eV, in good agreement with the experimental value of 2.0 ± 0.2 eV determined by Fomichev *et al.*[18] This is about the same as the value in 3C-SiC, where $E_g(\Gamma_{15v}$-$X_{1c}) = 2.39$ eV.

The lowest energy for direct transitions occurs at L, where the $L_{3v} - L_{1c}$ gap has an energy of 5.0 eV. This is one of the few differences between BP

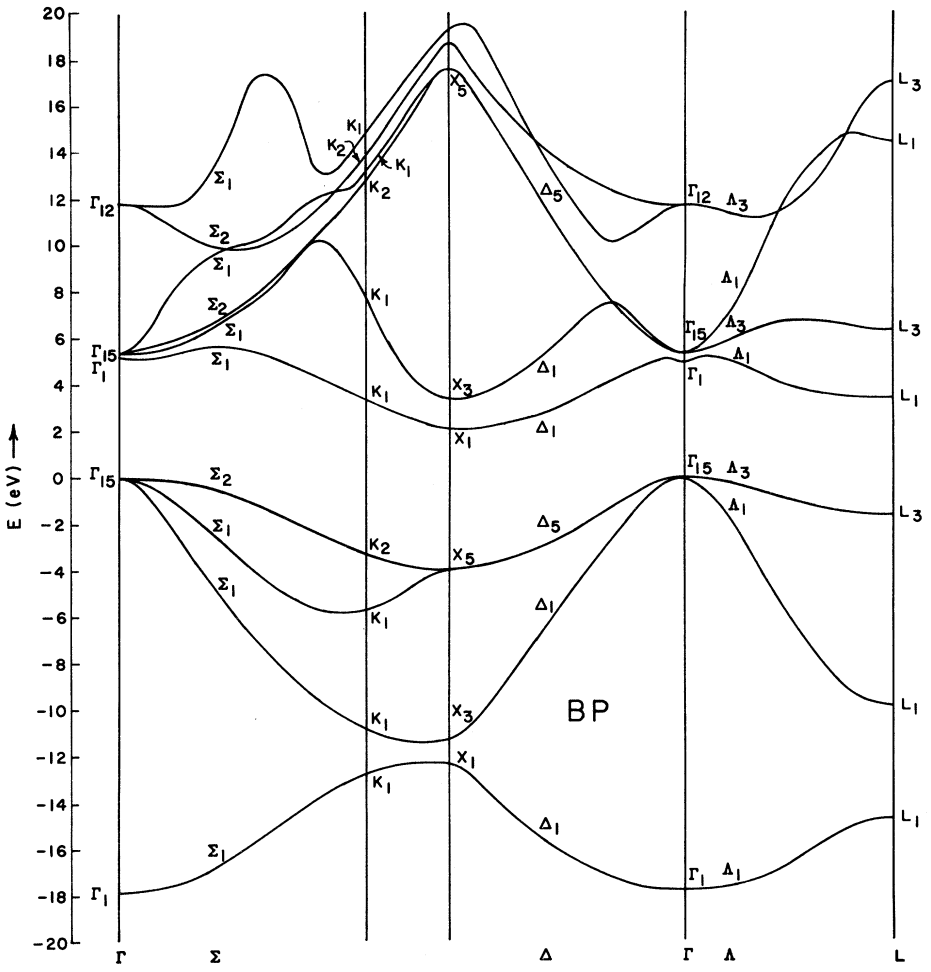

FIG. 8. Theoretical energy band structure of boron phosphide.

and 3C-SiC, where the direct gap is at Γ. However, the $\Gamma_{15v} - \Gamma_{1c}$ gap in BP is very near in energy at 5.25 eV, and small changes in the form factors (of less than 0.005 Ry) could easily effect a change in the direct gap of BP from L to Γ, without altering the remaining band structure significantly. Other than this minor difference, the band structures of BP and 3C-SiC are about the same. The ordering of the levels are identical, while the energy gaps of BP are all smaller than the corresponding gaps in 3C-SiC, as expected, since BP is less polar than SiC. This is indicated in Table II, where important band gaps in BP and 3C-SiC are compared.

The theoretical $\epsilon_2(\omega)$, derived from the band structure just discussed, is shown in Fig. 9. The reflectance $R(\omega)$ obtained via a Kramers-Kronig transformation of $\epsilon_2(\omega)$ is shown in Fig. 10, along with the experimental results of Wang *et al.*[19] Important energy contours and associated critical points are shown in Figs. 11 and 12 for 4 → 5 and 4 → 6 transitions, respectively.

The main features of the experimental $R(\omega)$ spectrum are a weak maximum at 5.0 eV, a main peak at 6.9 eV, and a shoulder near 8 eV. The calculated $R(\omega)$ has corresponding structure at 5.2, 7.0, and 7.7 eV, respectively. As noted in our discussion in Sec. III, the interband transitions responsible for these structures are most clearly determined by considering $\epsilon_2(\omega)$, whose shape can be directly connected to interband transitions occurring at critical points in the BZ.

The $\epsilon_2(\omega)$ spectrum of BP begins with direct transitions at L at an energy of 5.0 eV. The spectrum rises rapidly in this region due to the fact that the matrix elements are rather large, and there is a fairly large region in $\vec{k}$ space extending from L out along the Λ direction toward Γ where the valence and conduction bands are fairly parallel. In fact, at Γ the separation is still only 5.25 eV. Besides the M_0 critical point at L, corresponding to the $L_{3v} - L_{1c}$ transition, there are two other critical points in this region; an M_0 critical point at Γ associated with the $\Gamma_{15v} - \Gamma_{1c}$ transition of energy 5.27 eV, and an M_1 critical point at the position $(0.1, 0.1, 0.1)2\pi/a_{BP}$ along Λ of energy

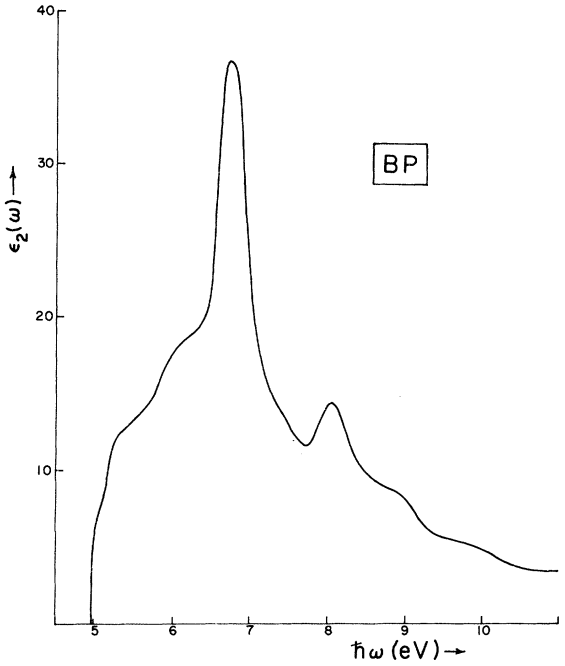

FIG. 9. Theoretical $\epsilon_2(\omega)$ of BP.

5.19 eV. Just above this region is another M_0 critical point at Γ corresponding to the $4 \rightarrow 6$ $\times \Gamma_{15v} - \Gamma_{15c}$ transition of energy 5.38 eV.

The main peak at 6.7 eV in $\epsilon_2(\omega)$, corresponding to the experimental peak at 6.9 eV in $R(\omega)$, has several contributions. First, there are two critical points associated with this structure: an M_1 critical point at X with energy 6.07 eV ($X_{5v} - X_{1c}$ transition), and an M_2 type singularity at the point (0.50, 0.50, 0)$2\pi/a_{BP}$ in the Σ direction, corresponding to the $\Sigma_{2v} - \Sigma_{1c}$ transition of energy 6.8 eV. In addition, there is a large volume contribution, especially in the ΓKWX plane, as shown in Fig. 11. As was seen in 3C-SiC and in diamond, the volume effect, i.e., contributions from a large region of $\vec{k}$ space, is a very important contribution to the prominent peak in III-V, IV-IV compounds and group-IV solids. Critical points at X and Σ often accompany such peaks, but are alone not sufficient to explain all such peaks; e.g., in 3C-SiC the critical peak at X is almost 1.5 eV below the main peak in energy, while diamond has no critical point at Σ.

As one goes higher in energy, $4 \rightarrow 6$ transitions become more important. Since the oscillator strengths for such transitions are usually smaller than those for $4 \rightarrow 5$ transitions, $\epsilon_2(\omega)$ falls smooth-

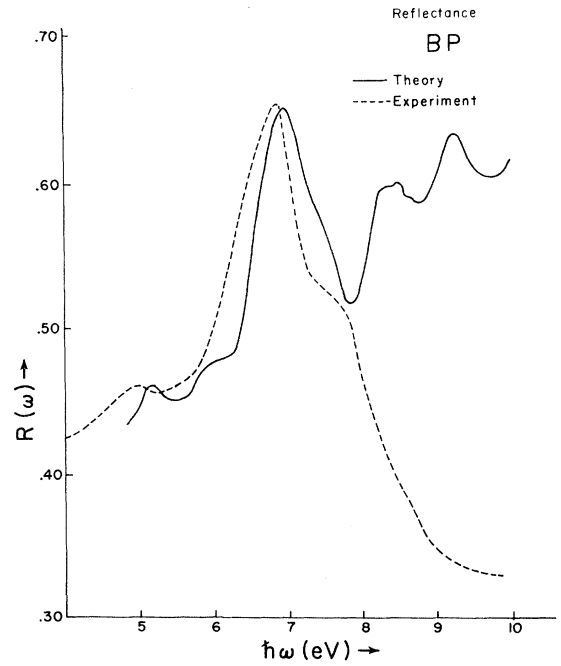

FIG. 10. Theoretical (full line) and experimental (dashed line) reflectance spectra of BP.

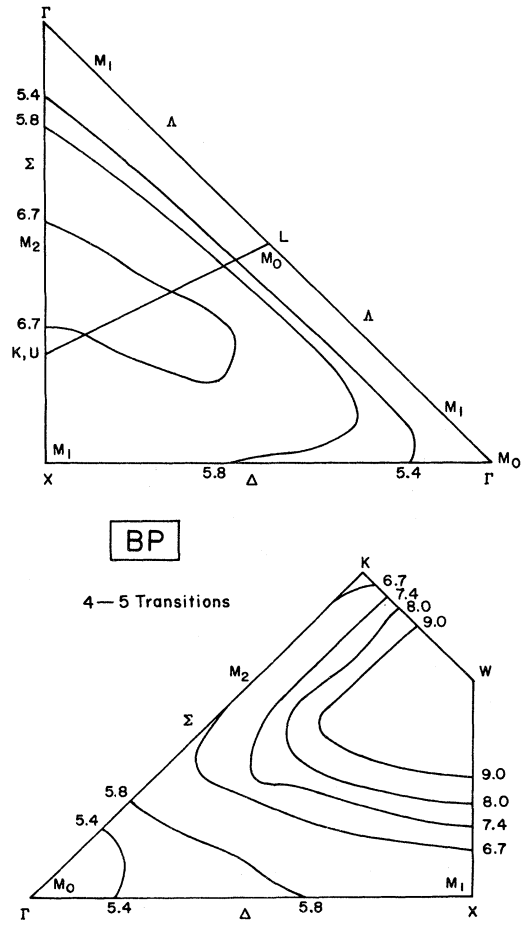

FIG. 11. Important BP energy contours and critical points for 4–5 transitions.

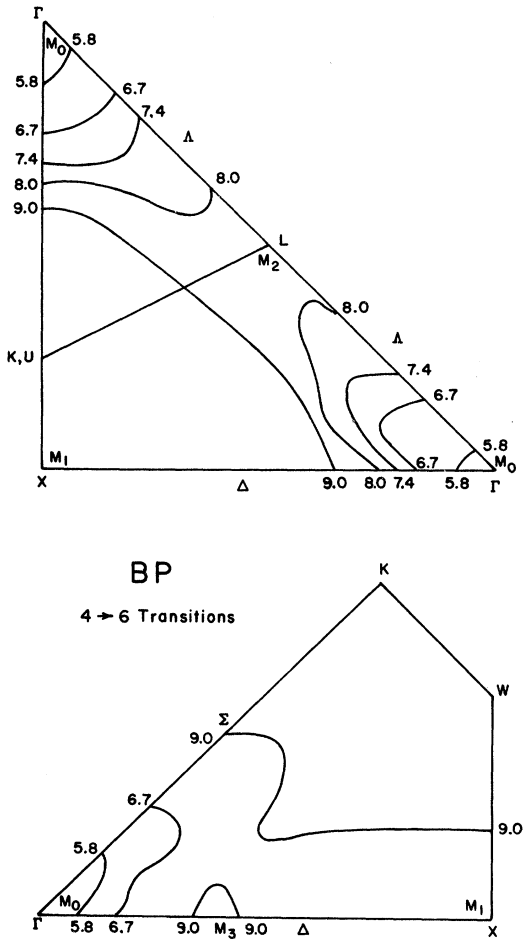

FIG. 12. Important BP energy contours and critical points for 4–6 transitions.

ly as energy increases, except near critical points. Above 7 eV, there is a critical point at X ($X_{5v} - X_{3c}$ transition) of the M_1 type with energy 7.35 eV, which contributes a very weak shoulder in $\epsilon_2(\omega)$ near 7.5 eV, an M_1 singularity at a general point in the BZ of energy 7.9 eV, as shown in Fig. 12, and an M_2 singularity near L at energy 8.02 eV ($L_{3v} - L_{3c}$ transition). These latter two critical points combine to give the peak at 8.0 eV in the calculated $\epsilon_2(\omega)$. Finally, there is a weak edge in $\epsilon_2(\omega)$ at 9 eV, corresponding to an M_3 critical point at the point $\Delta = (0.40, 0, 0)2\pi/a_{BP}$ in the BZ, corresponding to the $\Delta_{5v} - \Delta_{1c}$ transition of energy 9.04 eV. Above 10 eV, the experimental and theoretical $R(\omega)$ are quite different. However, the experimental measurements were made in 1962, and measurements at higher energies from that period of time are not very reliable. The structure in $R(\omega)$, along with the associated interband transitions and critical points is summarized in Table IV for convenience. The format is the same as that of Table III, corresponding to 3C-SiC, and is explained at the end of Sec. III.

In comparing Figs. 5 and 10, as well as Tables III and IV, one sees that the optical spectra and band structure of BP and 3C-SiC are quite similar, as are the interband transitions responsible for this structure. Both reflectance spectra exhibit peaks at low energies due to M_0 transitions near Γ and L, corresponding to the onset of direct interband transitions. Each spectrum is dominated by a single large peak, arising largely from $4 \rightarrow 5$ transitions in the region of the BZ near K and extending out along the Σ direction toward Γ and bending out along Δ toward the X-W boundary. Each also has a M_2 critical point near $(2\pi/a)$ (0.50, 0.50, 0) which contributes to the sharpness of this peak. Finally, both spectra have structure on the high-energy side of the main peak due to critical points associated with $4 \rightarrow 6$ transitions at X, L. Such general features tend to be characteristic of the optical spectra of III-V, II-VI, and group-IV solids studied thus far, reflecting a general over-all similarity in the band structure of these solids. The position of the optical structure in BP is generally lower than that of the corresponding structure in 3C-SiC due to the fact that BP is less polar then 3C-SiC, as discussed before, and hence should have correspondingly lower energy gaps (Table IV).

V. BORON NITRIDE

Just as it was convenient to think of BP as derived from 3C-SiC, one can likewise consider BN to be a perturbation on diamond with one carbon atom in the unit cell replaced by boron and the other replaced by nitrogen. One would then expect the symmetric form factors $V_S(G^2)$ to be roughly the same as the corresponding diamond form factors $V_C(G^2)$ (no scaling is required, since $a_{BN} \cong a_C$), while the antisymmetric form factors should be chosen to account for the difference in core charges between the boron and nitrogen ion cores. One can also define symmetric and antisymmetric nonlocal parameters A_S, A_A, given by

$$2A_S = A_B + A_N, \quad 2A_A = A_B - A_N,$$

where the subscripts B, N refer to boron and nitrogen, respectively. Then, by the same argument as above, one would expect $A_S \cong A_C$, the carbon value, whereas A_A could be chosen to account for differences between the two cores. The usual procedure, then, would be to allow the parameters $[V_A(3), V_A(4), V_A(11), A_A]$ to vary freely, keeping $[V_S(3), V_S(8), V_S(11), A_S]$ constant to within 0.02 Ry or so, until satisfactory agreement with the experimental data is achieved.

Unfortunately, such a procedure is not presently feasible for BN, since there is to date very little

TABLE IV. Summary of optical structure and associated critical points for BP. (See caption of Table III.)

Energy of optical structure (eV)		Associated critical points		
Expt.	Theoret.	Interband transition	Symmetry	Energy (eV)
5.0	5.0(5.2)	L_{3v}-L_{1c}	M_0	5.0
		Γ_{15v}-Γ_{1c}	M_0	5.25
6.9	6.7(7.0)	X_{5v}-X_{1c}	M_1	6.07
		Σ_{2v}-Σ_{1c}	M_2	6.8
8.0	8.1(8.05)	General point in BZ	M_1	7.9
		L_{3v}-L_{3c}	M_0	8.02

experimental data available. The only reference to the optical constants occurs in 1962 when Philipp and Taft[20] mention, in their paper on the optical properties of diamond, that "crude" reflectance measurements had also been made on BN, showing structure in the 9–10-eV region and a main peak is at least consistent with the dielectric calculation of Phillips,[21] who uses a generalization of Penn's two-band model along with the measured value of the static dielectric constant to determine a value of $E_g = 14.2$ eV for the main peak in $\epsilon_2(\omega)$. Additional experimental data is provided by Fomichev and Rumsch,[22] who report an upper limit to the width of the energy gap as 6.0 ± 0.5 eV and a lower limit to the valence bandwidth as 15.4 ± 0.5 eV. However, the former is at variance with the measurements of Gielesse *et al.*, who claim an energy gap of approximately 8 eV, while the latter figure of 15.4 eV could change to ≈ 22 eV with a different interpretation of the experimental data, as explained by the authors themselves. Previous calculations[23–25] are of no help in resolving these questions, as the calculated energy gaps range from 2.9 to 10.5 eV, while calculated valence-band widths span the range 12.6–23.5 eV. The net result of all this is that there is not enough reliable data which one can use to fix the parameters $[V_A(G^2), A_A]$ in the usual way.

In light of the scarcity of information concerning BN, we have been forced to make some rather drastic aasumptions in fixing the parameters $[V_A(G^2)\, A_A]$. The local antisymmetric form factors $V_A(G^2)$ are determined by taking the corresponding BP antisymmetric form factors and scaling them by a factor of $(a_{\mathrm{BP}}/a_{\mathrm{BN}})^3 \approx 2$ to account for the difference in lattice size between BN and BP. No further adjustment is made. By assuming $A_{\mathrm{B}} \approx A_{\mathrm{N}}$, A_A is set to be zero. *A priori*, it is hard to estimate how valid these approximations are. Lattice reflectivity measurements indicate that BN is the most ionic of all the III-V compounds, while BP is the least ionic solid in this class. Hence, one expects the BN form factors to be much larger than those of BP. It is unlikely that the factor of 2, introduced by the scaling procedure, wholly compensates for this difference, but it does, at least, partially do so. Moreover, the symmetric form factors $[V_S(G^2)]$ are the most important parameters in determining the band structure and optical properties, and these should be fairly accurately given by the diamond values. Hence, one would expect that the choice of parameters just outlined should give at least a rough first approximation to the band structure of BN, which could be improved by adjustments in the $[V_A(G^2), A_A]$ when more experimental data become available. This is the procedure we have adopted, and the resulting parameters are listed in Table I.

The band structure of BN is shown in Fig. 13. Like BP, the maximum of the valence band occurs at Γ_{15v}, while the conduction-band minimum occurs at either X or L, both of which have an energy of 7.60 eV above Γ_{15v}. The magnitude of the indirect gap tends more towards Gielisse's value of 8.0 eV than it does to the value of 6.0 to 6.5 eV quoted by Fomichev, but the location of the conduction band minimum in the BZ must await further experimental evidence. The band gap for direct transitions is 8.36 eV, corresponding to the $\Gamma_{15v} - \Gamma_{1c}$ transitions at Γ. Key energy gaps are listed in Table II, along with corresponding results for BP, 3C-SiC. In general, the gaps are larger for BN than they are for BP and 3C-SiC, which is in qualitative agreement with the fact that BN is the most polar of the three. The ordering of the levels in the three solids is essentially the same. The calculated BN valence bandwidth is 27.5 eV, which is much larger than even the largest minimal value of 22 eV quoted by Fomichev. This large valence bandwidth is no doubt due to the influence of the diamond form factors on BN, as the valence bandwidth of diamond was found to be close to 29 eV.[5] This indicates that the lowest lying valence band, which is unimportant for almost all properties especially optical ones, may lie too low in energy. If one includes only the three highest valence bands (i.e., bands 2–4), one finds a width of 16.5 eV, which seems quite consistent with previous calculations.[23–25]

The optical constants $\epsilon_2(\omega)$ and $R(\omega)$ of BN (Fig. 14) have also been calculated. However, we present only $\epsilon_2(\omega)$ in Fig. 14; $R(\omega)$ shows no additional

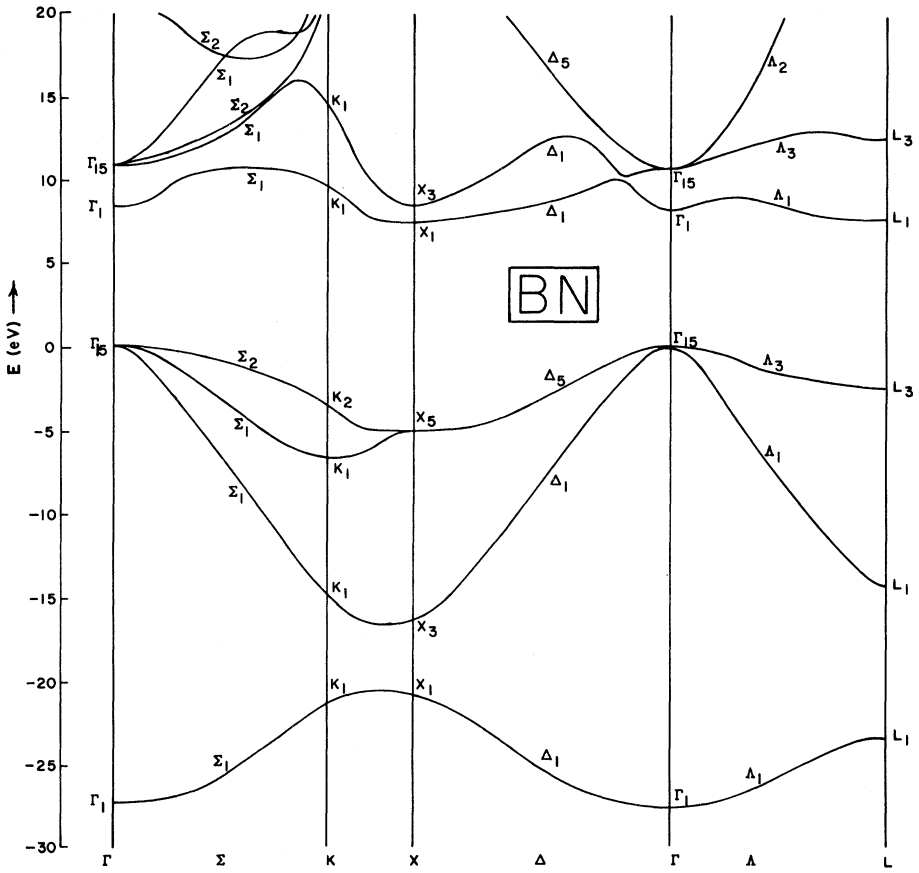

FIG. 13. Energy band structure of boron nitride.

structure, and there are no experimental data available to which it might be compared. It should be noted that, since the available experimental data are so coarse, we have performed only a very rough calculation of $\epsilon_2(\omega)$, using only about 250 000 sampling points in the BZ instead of the 10^6 or so

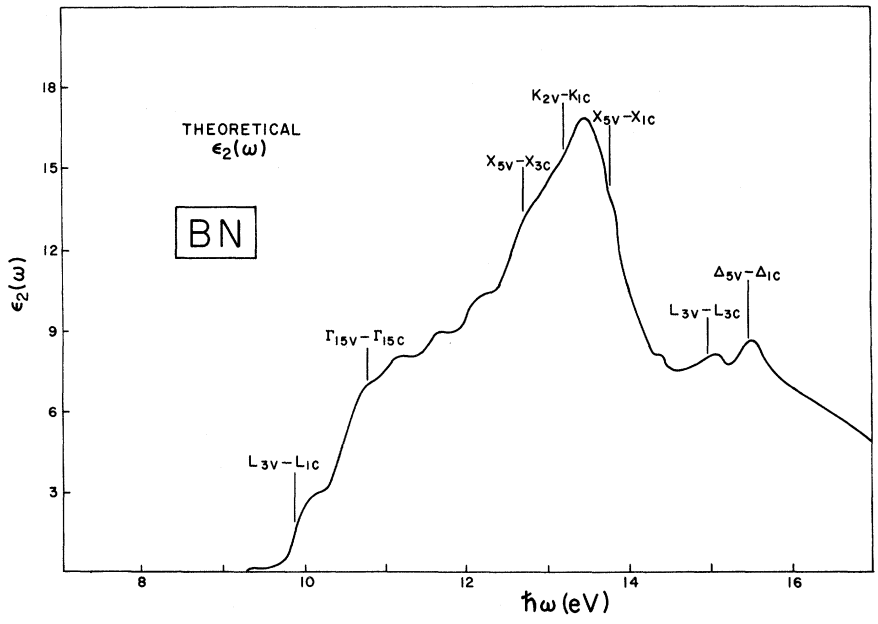

FIG. 14. Approximate $\epsilon_2(\omega)$ spectrum of BN.

TABLE V. Summary of calculated optical structure and associated critical points for BN. The theoretical energies listed are those occurring in the calculated $\epsilon_2(\omega)$ spectrum.

Energy of optical structure (eV)		Associated critical points		
Expt.	Theoret.	Interband transition	Symmetry	Energy (eV)
	8.4	Γ_{15v}-Γ_{1c}	M_0	8.36
	10.1	L_{3v}-L_{1c}	M_1	9.9
	10.8	Γ_{15v}-Γ_{15c}	M_0	10.8
	12.7	X_{5v}-X_{1c}	M_1	12.69
14.5	13.5	Volume effect		
	13.8	X_{5v}-X_{3c}	M_0	13.75
	15.1	L_{3v}-L_{3c}	M_1	14.95

used in calculating the spectra of BP and 3C-SiC. Such a sampling should reproduce the gross structure of $\epsilon_2(\omega)$ to within 0.3 eV or so, although additional spurious structure may result because of the coarseness of the mesh used, especially from regions in the BZ where the matrix elements vary rapidly.

The theoretical $\epsilon_2(\omega)$ begins with M_0-type transitions at Γ, corresponding to the $\Gamma_{15v} - \Gamma_{1c}$ energy gap of 8.36 eV. There is an M_1 critical point at L ($L_{3v} - L_{1c}$) of energy 9.9 eV, resulting in an edge at 10.1 eV, and an M_0 singularity at $\Gamma(\Gamma_{15v} - \Gamma_{15c})$ of energy 10.8 eV, associated with the edge at 10.8 eV in the spectrum. The edges at 11.2, 11.7, and 12 have no critical points associated with them, and are probably a result of the sampling procedure used. Similar structure below the main peak was found to occur in rough calculations of $\epsilon_2(\omega)$ for BP and 3C-SiC, only to disappear as more sampling points were employed. The shoulder in $\epsilon_2(\omega)$ near 12.7 eV is due to the $X_{5v} - X_{1c}$ transition of energy 12.69 eV, which represents a critical point of the M_1 type (Table V).

The main peak in $\epsilon_2(\omega)$ is situated at 13.5 eV. This is to be compared to the rough value of 14.5 eV given by Phillipp and Taft.[20] Actually, 14.5 eV refers to the reflectivity spectrum, whose main peak is generally 0.1–0.5 eV higher than the corresponding peak in $\epsilon_2(\omega)$. Hence, the agreement must be considered satisfactory, especially in view of the crudeness in both the experimental data and in the present calculation. There are no critical points associated with this peak, other than the M_0 critical point at X with energy 12.69 already discussed, with the main contribution coming from $4 \rightarrow 5$ transitions in the region of K extending in the Σ direction toward Γ, and then out along Δ to X, as discussed previously in Secs. III and IV. The shoulder at 13.8 eV on the high-energy side of the main peak can be assigned to the M_0 singularity at X ($X_{5v} - X_{3c}$ transition) of energy 13.75 eV, while the small edge at 14.4 eV has no associated critical point. The peaks at 15.1 and 15.5 can be assigned to an M_1 singularity at L due to the $4 \rightarrow 6$ transition $L_{3v} - L_{3c}$ of energy 14.95 eV and an inflection point near $2\pi/a(0.50, 0, 0)$, which acts as a weak pair of M_0 and M_1 critical points at energy 15.47 eV (Fig. 15).

Despite the rather drastic assumptions made in determining the parameters $V_A(G^2)$, A_A for BN, the resulting band structure does seem to yield a reasonable, although rough, first approximation to the real result. The band gap is close to the value quoted by Gielesse, and within 1 eV or so of that given by Fomichev. The main peak in $\epsilon_2(\omega)$ is within 0.5–1.0 eV of the value crudely determined by Philipp and Taft, and the $\epsilon_2(\omega)$ spectrum shows structure in the range 10–11 eV, probably corresponding to the structure in the 9–10-eV region reported by Philipp and Taft. The valence bandwidth may be too large, probably due to the fact that band one lies so low in energy, but this is a relatively unimportant feature as far as most physical properties go. The band structure near the fundamental gap of BN reported here is probably accurate to within 1 eV or so, and if new experimental data should become available, appropriate increases in $V_A(G^2)$, A_A should be able to improve this accuracy considerably.

Before leaving BN, it should be noted that we have also calculated energy bands at the symmetry points Γ, X, L, K without using V_{NL}. The effect of V_{NL} is found to be larger in BN than in either SiC or BP, but smaller than in diamond. The largest energy shift in band 4 occurs at X, where X_{5v} is shifted up by 0.5 eV or so by V_{NL}. This is to be compared to shifts of 0.15 to 0.25 in BP and 3C-SiC and the shift of 0.75 eV at X_4 in diamond. The reason why the shift in BN is smaller than that in diamond is probably due to the fact that the antisymmetric form factors tend to compensate part of the nonlocal effect. The antisymmetric potential arises from the difference in core charge between boron and nitrogen, and is attractive about nitrogen and repulsive about boron. The nonlocal potential, on the other hand, is attractive in both cases. These two contributions tend to compensate each other about the nitrogen cores.

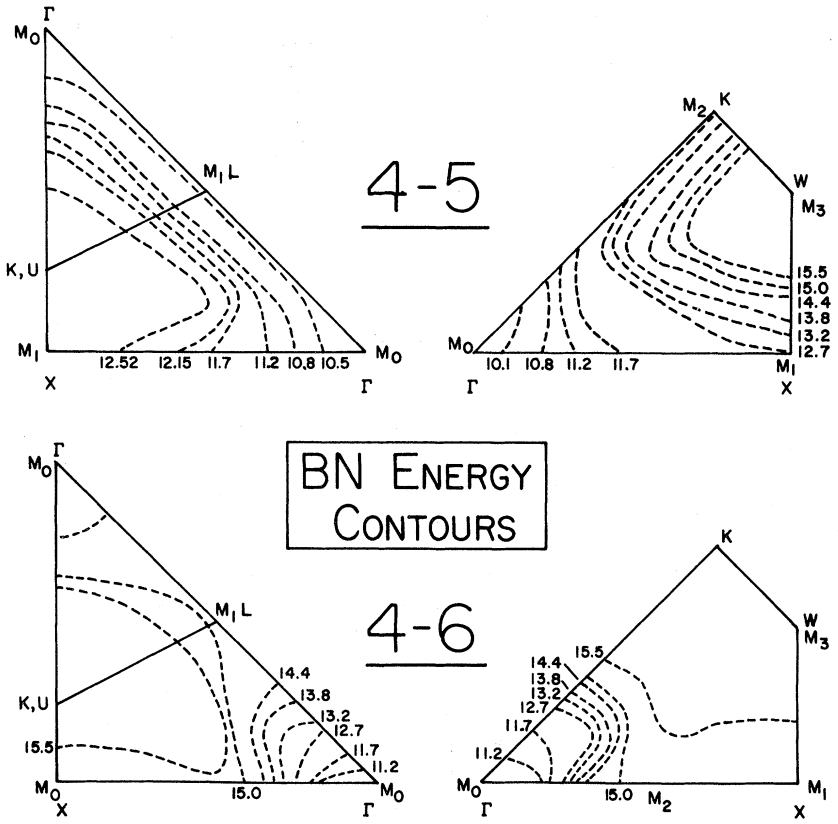

FIG. 15. Important BN energy contours and critical points for 4–5 and 4–6 transitions.

Hence, one expects V_{NL} to have an effect in BN intermediate between that in diamond, which gets strong contributions from all ion cores in the unit cell, and 3*C*-SiC or BP, which get contributions from only one-half of the ion cores.

VI. CONCLUSIONS

As seen in Sec. III–V, the NEPM seems to give quite reasonable results for the band structures of 3*C*-SiC, BP, and BN, as reflected in the agreement between the experimental optical data and that calculated on the basis of the computed band structure. Even BN, for which some rather questionable assumptions were introduced, seems to be at least reasonably consistent with the scarce and sometimes conflicting experimental data. Actually, as was discussed in Secs. III–IV, the nonlocal term V_{NL} is not as important in SiC and BP as it is in diamond and BN, and the former solids could probably have been adequately handled using the usual local EPM method. Such a nonlocal term is essential if one is to accurately reproduce the optical data of diamond and BN, however. It is hoped that further experimental evidence on BN will be forthcoming in the future so that our NEPM results can be improved. We notice that the $V_A(3)$'s are smaller than the $V_A(4)$'s in these three compounds. This may be related to the covalent nature of these compounds. We shall not go into the details in this paper.

ACKNOWLEDGMENTS

We would like to thank Dr. W. J. Choyke for sending some preliminary reflectance data on 3*C*-SiC. Thanks are due Professor Marvin L. Cohen for several helpful comments on the manuscript. This research was partially funded by the Committee on Research at the University of California, Davis.

*Present address: Department of Physics, Polytechnic Institute of Brooklyn, Brooklyn, New York 11201.

[1]M. L. Cohen and V. Heine, in *Solid State Physics* (Academic, New York, 1970), Vol. 24, pp. 37–248.

[2]V. Heine, in *Solid State Physics*, edited by F. Seitz and D. Turnbull (Academic, New York, 1970), Vol. 24, pp. 1–36.

[3]W. Saslow, T. K. Bergstresser, and M. L. Cohen, Phys. Rev. Letters 16, 354 (1966).

[4]L. Saravia and D. Brust, Phys. Rev. 170, 683 (1968).

[5]L. A. Hemstreet, C. Y. Fong, and M. L. Cohen, Phys. Rev. B 2, 2054 (1970); hereafter to be referred to as HFC.

[6]L. A. Hemstreet and C. Y. Fong, Solid State Commun.

9, 643 (1971); hereafter to be referred to as I.
[7]R. H. Parmenter, Phys. Rev. 100, 573 (1955).
[8]D. Brust, Phys. Rev. 134, A1337 (1964).
[9]J. Walter and M. L. Cohen, Phys. Rev. 183, 763 (1969).
[10]J. C. Phillips, in Ref. 2, Vol. 18, pp. 55–164.
[11]W. J. Choyke, D. R. Hamilton, and Lyle Patrick, Phys. Rev. 133, A1163 (1964).
[12]B. E. Wheeler, Solid State Commun. 4, 173 (1966).
[13]W. J. Choyke and L. Patrick, Phys. Rev. 187, 1041 (1969).
[14]M. L. Belle, N. K. Prokof'eva, and M. B. Reifman, Sov. Phys. Semicond. 1, 315 (1967).
[51]F. Herman, J. P. Van Dyke, and R. L. Kortum, Mater. Res. Bull. 4, S167 (1969).
[16]P. J. Gielisse, S. S. Mitra, J. N. Plendl, R. D. Griffis, L. C. Mansur, R. Marshall, and E. A. Pascoe, Phys. Rev. 155, 1039 (1967).
[17]J. C. Phillips, Rev. Mod. Phys. 42, 317 (1970); J. A. Van Vechten, Phys. Rev. 182, 891 (1969); 187, 1007 (1969).
[18]V. A. Fomichev, I. I. Zhukova, and I. K. Polushina, J. Phys. Chem. Solids 29, 1025 (1968).
[19]C. C. Wang, M. Cardona, and A. G. Fischer, RCA Rev. 25, 159 (1964).
[20]H. Philipp and E. A. Taft, Phys. Rev. 127, 159 (1962).
[21]J. C. Phillips, J. Chem. Phys. 48, 5740 (1968).
[22]V. A. Fomichev and M.A. Rumsch, J. Phys. Chem. Solids 29, 1015 (1968).
[23]Reported as a private communication in the paper on the energy bands of BN, D. R. Wiff and R. Keown, J. Chem. Phys. 47, 3113 (1967).
[24]L. Kleinman and J. C. Phillips, Phys. Rev. 117, 460 (1959).
[25]F. Bassini and M. Yoshimine, Phys. Rev. 130, 20 (1963).

PHYSICAL REVIEW B VOLUME 6, NUMBER 4 15 AUGUST 1972

Optic Modes in Amorphous As_2S_3 and As_2Se_3

G. Lucovsky
Xerox Palo Alto Research Center, Palo Alto, California 94304
(Received 27 March 1972)

New reflectance spectra are obtained for amorphous As_2S_3 and As_2Se_3. The spectra contain features not reported in earlier studies. Analysis of the spectra in terms of damped Lorentzian oscillators, combined with new Raman data, gives further support to the validity of a molecular model for the optic-mode vibrational frequencies. Using mode masses derived from the model, values of the macroscopic effective charge e_T^* are obtained. For both materials, e_T^* values are comparable to those of other covalently bound solids; e.g., trigonal Se and trigonal Te. Contrary to early suggestions, it is demonstrated that the large values of e_T^* in these materials are not a manifestation of ionic bonding but rather result from dynamical charge transfer. In both As_2S_3 and As_2Se_3 there are sufficient differences between the infrared (ir) and Raman spectra so that they cannot be interpreted simply in terms of a density of states by assuming a complete breakdown of selection rules due to disorder. On the contrary, selection rules resulting from the short-range order or the molecular nature of these solids are of considerable importance in determining the ir or Raman activity of the optic modes.

I. INTRODUCTION

The first report of reststrahlen bands in chalcogenide glasses was made by Hilton *et al.*[1] Felty, Lucovsky, and Myers[2] studied the dominant reststrahlen band in both As_2S_3 (at ~300 cm^{-1}) and As_2Se_3 (at ~220 cm^{-1}) and found that this band displayed a two-mode behavior[3] in the pseudobinary alloy system $As_2S_{3-x}Se_x$ analogous to that reported for crystalline alloy systems, e.g., $CdS_{1-x}Se_x$. Taylor, Bishop, and Mitchell[4] studied As_2Se_3 in greater detail. They identified a second and weaker reststrahlen (at ~100 cm^{-1}) and studied the absorption spectrum as well. They found that a Gaussian line shape gave a better fit to the wings of the absorption bands than did a Lorentzian line shape. Infrared (ir) reflectance bands in crystalline materials have traditionally been fit with damped Lorentzian oscillators. Zlatkin and Markov[5] studied both crystalline and amorphous As_2S_3 and As_2Se_3. They calculated values of the Szigeti effective charge e_s^* for the amorphous materials and suggested that the large values of e_s^* they found, $0.94e$ for As_2S_3 and $0.67e$ for As_2Se_3, were indicative of a substantial ionic content to the chemical bonding. Onomichi, Arai, and Kudo[6] also studied amorphous As_2S_3 and As_2Se_3 and reported similar values for e_s^*. The Raman spectrum of As_2S_3 was studied by Ward and Myers[7] and by Kobliska and Solin[8] and that of As_2Se_3 by Schottmiller *et al.*[9] A comparison of the ir and Raman data indicated that the frequencies of the dominant modes are different.[10]

In this paper we present new reflectance spectra for As_2S_3 and As_2Se_3 in the region of the dominant reststrahlen bands, 180–450 cm^{-1}. In the earlier